Fluid Dynamics & Materials Processing

Tech Science Press

DOI: 10.32604/fdmp.2022.019719

ARTICLE

An Analysis of the Formation Mechanisms of Abrasive Particles and Their Effects on Cutting Efficiency

Wei Zhang*

Research Center of Mould Precision Machining & Intelligent Manufacturing Application, Ningbo Polytechnic, Ningbo, 315800, China

*Corresponding Author: Wei Zhang. Email: zw111150@163.com

Received: 10 October 2021 Accepted: 16 February 2022

ABSTRACT

Magnetic induction-free abrasive wire sawing (MIFAWS) is a method that combines magnetic fields with traditional free abrasive wire sawing technologies. Magnetic abrasive particles (MAPs) are attracted on a magnetized wire, thus leading to an increase in their number into the cutting zone. The number of instantaneous-effective abrasive particles (IEAPs) adsorbed on the wire surface has a great influence on the cutting efficiency of the saw wire. In this study, a mathematic model of the movement of the MAP is presented, and the factors influencing the IEAPs number, including slurry-supply speed and slurry dynamic viscosity, are investigated both by means of simulation analysis and experiments. The results indicate that the number of IEAPs decreases with an increase in the slurry supply speed. The cutting efficiency increases gradually with the increase of slurry supply speed, but the growth rate of wire saw cutting efficiency slows down when the slurry supply speed exceeds a given threshold. The number of IEAPs adsorbed by saw wire increases with a decrease in the dynamic viscosity of the cutting fluid, while the cutting efficiency first increases and then decreases. The cutting efficiency attains its highest value when the dynamic viscosity of the cutting fluid is 0.0047 Pa·s. The experimental results agree with the simulation results, and provide some guidance for the practical application of the MIFAWS process.

KEYWORDS

Instantaneous-effective abrasive particle; magnetic field; adsorption; wire sawing; cutting efficiency

1 Introduction

Silicon wafers serve as substrates for solar cells. Slicing is a key process in the fabrication of silicon wafers. Its cost accounts for about 20% of the manufacturing costs of solar cells [1–3]. With rapid development of the photovoltaic and semiconductor industries, the dimensionality of silicon wafers is generally required to be large and thin. This need hence requires higher degrees of fidelity and precision within silicon wafer cutting processes [4,5]. Free and fixed-abrasive wire sawing approaches are the most widely utilized in industry for silicon wafer preparation. Diamond wires used in the fixed-abrasive wire sawing process are more expensive than the steel wires typically used in the free-abrasive wire sawing process. The former type of wire (diamond) removes materials mainly through a "scratch" process, often leading to great extent of damage on the wafers. This disadvantage significantly limits its application within the silicon (especially polysilicon) slicing process [6,7]. Free-abrasive wire sawing, however, is a

current leading technology for slicing polysilicon ingots into wafers because of its small kerf loss, good surface quality, and the ability to cut ingots of large size. It removes materials mainly through a three-body wear method [8]. Overwhelmingly, silicon slicing technologies that exhibit higher cutting efficiencies and lower cutting expenses are most sought after in the manufacturing sector. Accordingly, a considerable degree of research to improve the free-abrasive wire sawing process has been conducted over recent years. Bhagavat et al. [9] studied the influence of multiple simultaneous indentations on a material's response using the finite element method. The study's results showed that indentation depth generally increases as the spacing between abrasive particles decreases. Hence, material removal rates increase (for a given load) as spacing between abrasives decrease. Schwinde et al. [10] investigated wire behavior during multi-wire sawing at commercial facilities utilized for large-scale production. The results revealed that material removal occurred primarily only on one side of the wire. In order to reduce kerf loss and wire consumption, a wire with a non-circular cross-section was subsequently proposed. As a result, cost-effectiveness for solar cells was ultimately achieved. Such a wire design; however, is much more difficult to prepare than a traditional wire. Nassauer et al. [11] studied the mechanism of wire sawing at the micro-level both by numerical simulation and through experimental trial. The results showed that the number of involved particles was very low. Bao et al. proposed a new technique called "abrasive electrochemical multi-wire slicing" (AEMS), which combines the functions of electrochemical reactions and mechanical grinding. Per this approach, the surface integrity and slicing efficiency were found to improve significantly. However, the deployment of the AEMS technique does have an inherent drawback in the way of large electrical power demand which therefore limits its extent of viable use and application within numerous wire sawing industrial settings [12].

A method of free-abrasive wire sawing which facilitates the wire being able to transport more abrasive grains into the sawing channel without changing machining parameters, wire surface characteristics, etc., is presently lacking. Our proposed method, referred to as "magnetic induction free-abrasive wire sawing" (MIFAWS), applies an external uniform magnetic field around the ferromagnetic wire during the sawing process. In MIFAWS, a large number of magnetic abrasive particles (MAPs) are collected on the wire surface by the magnetic force of the magnetized wire. Resultantly, a larger number of abrasive particles are attracted into the sawing channel between the wire and workpiece thereby improving overall wire sawing performance. This novel method is similar to "Magnetic Abrasive Finishing" technology, wherein magnetic abrasives are accumulated by magnetic forces and resultantly forma flexible magnetic abrasive brush [13]. The number of MAPs that ultimately enter the cutting area has a major impact on wire sawing performance. In this paper, to further elucidate the mechanism of the MIFAWS method, we comprehensively analyze the forces acting upon a wire's MAPs. A dynamic model of abrasive particles was then established by comprehensively considering the magnetic forces and fluid drag forces acting on the particles. The effects of slurry-supply speed and slurry dynamic viscosity on the instantaneous-effective abrasive particle (IEAP) number under a certain magnetic field strength were simulated using finite element methods. Finally, adsorption experiments and cutting experiments were performed to verify simulation results.

2 Materials and Methods

2.1 Force Analysis of MAPs

Based on the wire sawing process, a geometric model indicates that the MAPs motion around the single-wire is configured as shown in Fig. 1 below. The rectangular area denotes the slurry flow area, and the middle small circle represents the saw wire. Considering the single-wire is infinitely long, it is reasonable to ignore the change of each physical quantity along the axis. The wire saw used for free-abrasive wire cutting is comprised of copper-plated steel. As a kind of ferromagnetic material, it will be magnetized in a uniform magnetic field to produce a high-gradient magnetic field. The field has a magnetic effect on the

surrounding MAPs. The slurry was made from a proportioned mixture of polyethylene glycol 300 (PEG300) and nickel-plated silicon carbide (SiC). Compared with the traditional free-abrasive wire sawing process, a larger number of abrasive particles will be adsorbed on the saw wire surface (i.e., IEAPs), and ultimately brought into the cutting area under magnetic forces. Hence, the number of effective abrasive particles in the cutting area increases, causing an overall marked improvement in wire sawing performance.

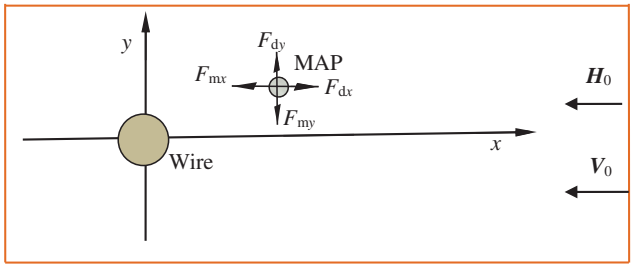

Figure 1: Force analysis of MAPs

This paper mainly considers the two-dimensional bounded flow of MAPs in the slurry. We regard the slurry as a continuous medium and the MAPs as a discrete system. To facilitate the dynamic analysis, the MAPs were considered spherical. The MAPs move to the non-cutting area by the action of the fluid. The magnetic force (F_m) and drag force (F_d) acting on the MAPs are primarily taken into consideration for this study. A uniform magnetic field was considered without any external electric field in play. The magnetization of the wire is denoted by M, paralleling to the background magnetic field. Accordingly, the magnetic potential (V_m) can be expressed using the Laplace equation as follows [14,15]:

$$\nabla V_m = 0 \tag{1}$$

The model comprises two regions with different magnetic properties: a strong magnetic region and a weak magnetic region. Magnetic potential is denoted by V_{m1} and V_{m2}, which can be expressed using the Laplace equation as:

$$\nabla V_{m1} = 0 \tag{2}$$

$$\nabla V_{m2} = 0 \tag{3}$$

Hence, the magnetic induction of the wire and other regions can be obtained as follows:

$$B_1 = -\mu_0\left(\frac{\partial V_m}{\partial x}, \frac{\partial V_m}{\partial y}\right) = \mu_0\left((M + H_0) - \frac{\partial V_{m1}}{\partial x}, -\frac{\partial V_{m1}}{\partial y}\right) \tag{4}$$

$$B_2 = -\mu_0\left(\frac{\partial V_m}{\partial x}, \frac{\partial V_m}{\partial y}\right) = \mu_0\left(H_0 - \frac{\partial V_{m2}}{\partial x}, -\frac{\partial V_{m2}}{\partial y}\right) \tag{5}$$

where $\boldsymbol{H}_0$ is the external magnetic field strength, μ_0 is the vacuum permeability, and M is the magnetization intensity of the wire measured by a vibrating sample magnetometer (Lake Shore VSM 7307).

The magnetic field strength ($\boldsymbol{H}$) at the location of the MAPs is thus determined via the following:

$$H = \sqrt{H*H} = \left[\left(H_0 - \frac{\partial V_{m2}}{\partial x}\right)^2 + \left(-\frac{\partial V_{m2}}{\partial y}\right)^2\right]^{\frac{1}{2}} \tag{6}$$

$$F_m = 2\pi r_p^3 \mu_0 \mu_r K V_p \nabla(H^2) \tag{7}$$

where $K = \frac{\mu_{r,p} - \mu_r}{\mu_{r,p} + 2\mu_r}$. Here, $\mu_{r,\,p}$ and μ_r are therelative magnetic permeability and magnetic permeability of the MAPs, respectively, and K is the difference in magnetic susceptibility between the MAPs and the fluid.

In this study, the fluid Reynolds number is low in the Stokes' law area, and the fluid is considered incompressible. Hence, the fluid drag acting on the abrasive particles can be expressed using Stokes' law as [16]:

$$F_d = -\frac{1}{\tau_p} m_p (u_p - u), \quad \text{where} \quad \tau_p = \frac{\rho_p d_p^2}{18\eta} \tag{8}$$

Here, u and u_p are the slurry velocity and abrasive particle velocity at the abrasive particle's position, respectively, and η is the slurry dynamic viscosity.

The associated equation of motion is based on Newton's second law:

$$F_d + F_m = ma \tag{9}$$

Substituting Eqs. (7) and (8) into Eq. (9), the movement of MAPs is functionally related to slurry-supply speed, slurry dynamic viscosity, external uniform magnetic field strength, and relative magnetic permeability. At this juncture, IEAP formation mechanisms can now be evaluated using finite element methods.

2.2 Simulation Model and Parameters

The formation of IEAPs in the fluid was modeled by the commercial software COMSOL Multiphysics, a specialized software module that analyzes multi-field coupling problems. The model in Fig. 1 was constructed as a simplified 2D representation along the wire diameter direction (x-axis). The model was meshed into triangular elements, which were refined around the wire for high-precision computations within the region of importance. The fluid flow was modeled as laminar flow entering the model at an assigned initial velocity from the velocity inlet boundary. The laminar flow, however, was subjected to wall boundary conditions at the wire interface. All interfaces in contact with the fluid stream were subjected to no-slip boundary conditions. The magnetic abrasive grains were released from the inlet at the same initial velocity as the fluid; initially, they moved in a direction perpendicular to the velocity inlet boundary. A listing of all applicable parameters employed within this simulation is provided below in Table 1.

Table 1: Simulation parameters

Parameter	Numerical values
Fluid initial velocity (mm/s)	16, 12, 8, and 4
Abrasive particle mean diameter (μm)	25
Wire radius (mm)	0.2
Magnetic permeability (H/m)	1.0726
Fluid viscosity (Pa·s)	0.0400, 0.0165, 0.0047, and 0.0017
Magnetic field intensity (A/m)	9.54×10^4
Magnetic permeability of wire (H/m)	11.4

2.3 Observing Experiment Device and Parameters

Due to the inherent difficulties of observing IEAPs formed on wire surfaces, we constructed an experimental platform to model the wire sawing process along the wire cross-section direction, as illustrated below in Fig. 2. A magnetic system containing permanent magnets and highly magnetic conductive materials was designed and manufactured based on the magnetic circuit design principle [17]. The magnetic system should not only provide a high magnetic field strength but should also meet the practical application specifically tailored for a single-wire sawing machine. A steel wire was placed in the center of the system and was fixed utilizing a device manufactured by 3D-printing technology. The device was then injected with a slurry of PEG300 fluid and nickel-plated SiC through the slurry entrance. Magnetic induction intensities were varied by adjusting the differential gaps within the system and were measured by a Gauss-meter HT201 at the wire's position. PEG300 cannot decompose directly in the natural environment. It will cause serious environmental pollution if freely discharged, and manual decomposition techniques exhibit considerable processing challenges and large financial expenditures. Therefore, it is of great significance to evaluate the influence of dynamic viscosity on IEAP number. The selected mass fractions of PEG300 for this evaluation were 25%, 50%, 75%, and 100%, and the corresponding dynamic viscosities of the slurry were 0.0017 Pa·s, 0.0047 Pa·s, 0.0165 Pa·s, and 0.04 Pa·s, respectively. Dynamic viscosity was measured using a digital viscometer (NDJ-9S, Shanghai) at room temperature. The slurry wastes a lot if the slurry-supply speed was large, while it cannot meet the supply requirements if the slurry-supply speed was small. So the selected slurry-supply speeds in this paper were 16, 12, 8, and 4 mm/s. these explanations have been added in our revised paper. In this experiment, the slurry was supplied to the platform through the slurry entrance at differing speeds. The mass fraction of the nickel-plated SiC particles was 1%, and the initial velocity of the slurry was controlled utilizing a peristaltic pump (LLs Plus, Kamoer Corporation). A high-speed camera (VW–6000/5000, Keyence Corporation) was then used, which was equipped with a lens placed above the wire at a magnification of 200× to record the formation of IEAPs on the wire surface. The listings of associated experimental parameters (and values) are provided in Table 2 below.

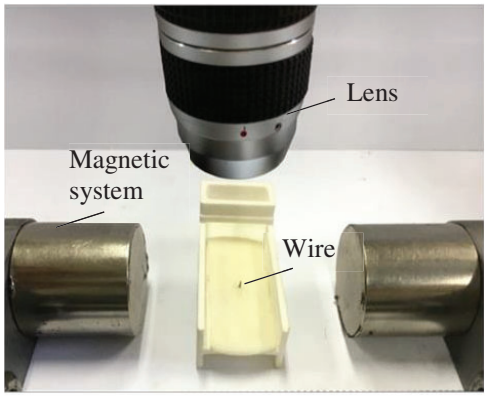

Figure 2: Experimental platform

2.4 Cutting Experiment Device and Parameters

To further study the influence of the number of IEAPs on wire sawing performance, a MIFAWS platform was built as shown in Fig. 3 below. It combined a magnetic system and a WXD170 reciprocating wire sawing machine (Shenyang Maike Material Processing Equipment Company, China). The slurry consisted of PEG300 and magnetic abrasive grains, with an abrasive grain concentration of 30%, which is a commonly used percentage in practical wire sawing processes. Nickel-plated SiC was used as the

magnetic abrasive grain material. A copper-coated steel wire with a diameter 0.4 mm was utilized. The workpiece was comprised of optical glass K9 with a size of 32 mm×32 mm×32 mm (32,768 mm^3). For one workpiece, three cuts were executed on a single-wire sawing machine. A uniform magnetic field was successfully created by the deployed magnetic system. The cutting experiment mainly includes three groups. For one work-piece, three cuts are executed using a single wire sawing machine, which takes 20 min for each group of optical glass. After each cut, the removed mass of the work-piece is weighed by an accurate electronic balance (Shanghai, ZA805S) to determine the cutting efficiency. The associated experimental parameters for this trial are provided below in Table 3.

Table 2: Experimental parameters

Parameter	Numerical values
Slurry-supply spped (mm/s)	16, 12, 8, and 4
Abrasive particle diameter (μm)	25
Diameter of saw wire (mm)	0.4
Fluid dynamic viscosity (Pa·s)	0.0400, 0.0165, 0.0047, and 0.0017
Magnetic field intensity (A/m)	9.54×10^4
Abrasive grains concentration	1%

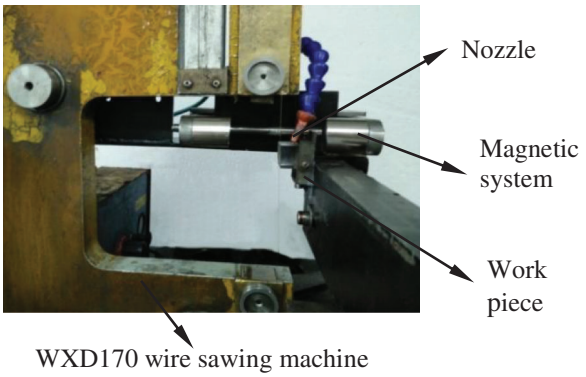

Figure 3: Platform of MIFAWS

Table 3: Cutting parameters

Parameters	Value
Diameter of saw wire (mm)	0.4
Mean diameter of abrasive grains (μm)	25
Wire speed (m/s)	2
Workpiece feed speed (mm/min)	0.5
Wire tension (MPa)	0.2
Abrasive grains concentration	30%

3 Results and Discussion

3.1 Simulation Results and Discussion

3.1.1 Effect of Slurry-Supply Speed on IEAP Number

Figs. 4 and 5 show the results of IEAP formation and quantity at different slurry-supply speeds (with a slurry dynamic viscosity of 0.04 Pa·s). It can be seen that the slurry-supply speed has a considerable influence on the IEAPs adsorbed by the saw wire. The quantity of IEAPs increases and the range becomes larger as the slurry-supply speed decreases. Saw wire in MIFAWS is magnetized by an external uniform magnetic field, producing magnetic forces on abrasive particles. Hence, a large number of MAPs are collected on the wire surface by the attractive forces. The magnetic forces of MAPs remain unchanged if the external magnetic field strength in play remains unchanged. The drag force of cutting fluid on abrasive particles is also very large when the slurry-supply speed is high. During such occasions, the drag force plays a major role in the movement of abrasive particles, and lesser number of particles are ultimately adsorbed around the saw wire to become IEAPs. When the slurry-supply speed is low, magnetic forces play a major role in the movement of abrasive particles. During such occasions, a higher quantity of abrasive particles are adsorbed around the saw wire and enter the cutting area with the saw wire, thus resulting in a net increase in the number of effective abrasive particles. It can be seen via Eq. (9) that the fluid drag force acting on MAPs decreases as slurry-supply speed increases. Hence, the lower the slurry-supply speed is, the more IEAPs are adsorbed on the saw wire. These results are experimentally verified in the following section.

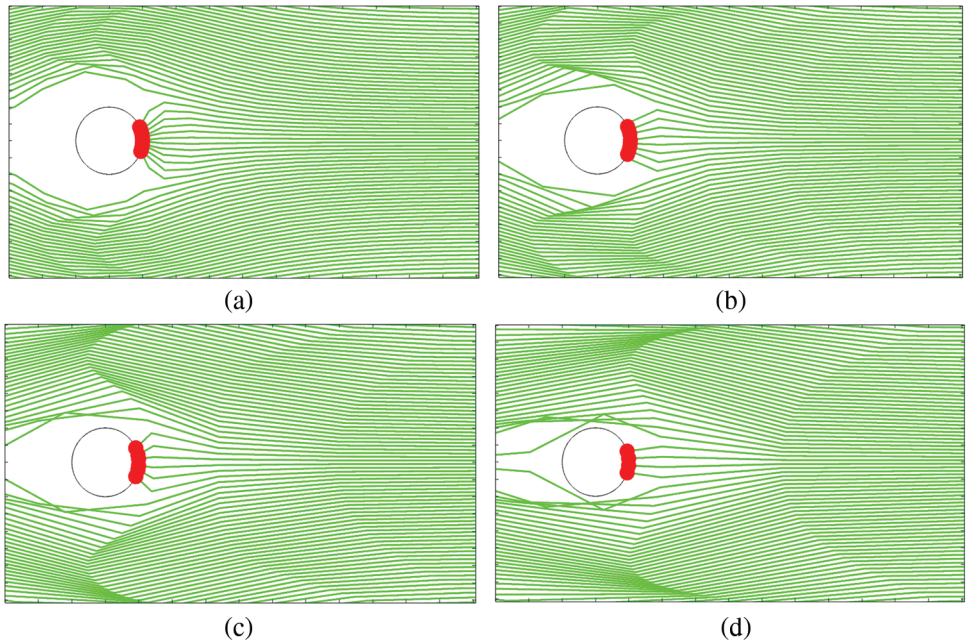

Figure 4: IEAPs formation at different slurry-supply speeds (a) V_0 = 4 mm/s, (b) V_0 = 8 mm/s, (c) V_0 = 12 mm/s (d) V_0 = 16 mm/s

Assuming that the release time step of a magnetic abrasive particle is 0.01 s when the slurry-supply speed is 10 mm/s, 100 abrasive particles will theoretically be released during a one-second interval. According to the relationship between the magnitude of slurry-supply speed and the frequency of releasing abrasive particles, the total number of effective abrasive particles adsorbed by saw wire under different slurry-supply speeds over a period of one-second is calculated, as shown below in Fig. 6.

12 mm/s (d) V_s= 16 mm/s.

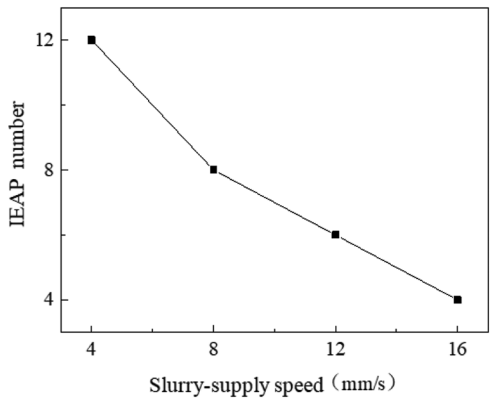

Figure 5: IEAP number at different slurry-supply speeds

As can be seen in the Fig. 6, as the slurry-supply speed increases, the total number of IEAPs adsorbed by the saw wire during a one-second interval initially increases and then drops off. The total number of effective abrasive particles is highest when the slurry-supply speed is 12 mm/s. This is mainly due to the notion that as the slurry-supply speed increases (commensurate with an associated increase of abrasive particle release frequency), the magnetic force of the gradient magnetic field remains constant, hence resulting in no change to the abrasive particle concentration within the slurry. This condition therefore facilitates a higher abrasive particle flow to the saw wire. Consequently, within a certain speed range, as the speed increases, a larger quantity of abrasive particles are adsorbed by the saw wire and become effective abrasive particles. When the slurry-supply speed is 4 mm/s, the number of IEAPs that are instantaneously adsorbed is at its maximum, but due to the low speed, the number of IEAPs adsorbed in one second (per unit time) is at its minimum.

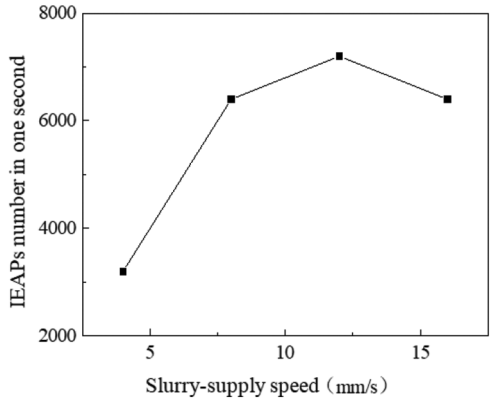

Figure 6: IEAPs number under different slurry-supply speeds in one second

3.1.2 Effect of Slurry Dynamic Viscosity on IEAP Number

Figs. 7 and 8 show the results of IEAP formation and number at different dynamic viscosities (with a slurry-supply speed of 4 mm/s). It can be seen that the number of IEAPs adsorbed by the saw wire decreases as dynamic viscosity increases. The greater the dynamic viscosity of the cutting fluid is, the greater the internal friction and drag forces of the fluid are when flowing at the same speed. In addition, drag forces on the MAPs decrease as the dynamic viscosity of the cutting fluid decreases. It also can be

seen from the distribution of abrasive particles adsorbed on the saw wire that the greater the dynamic viscosity of the cutting fluid, the higher the degree of particle dispersion there tends to be around the wire. Conversely, a lower cutting fluid dynamic viscosity generally correlates to a higher MAP concentration adsorbed around the wire.

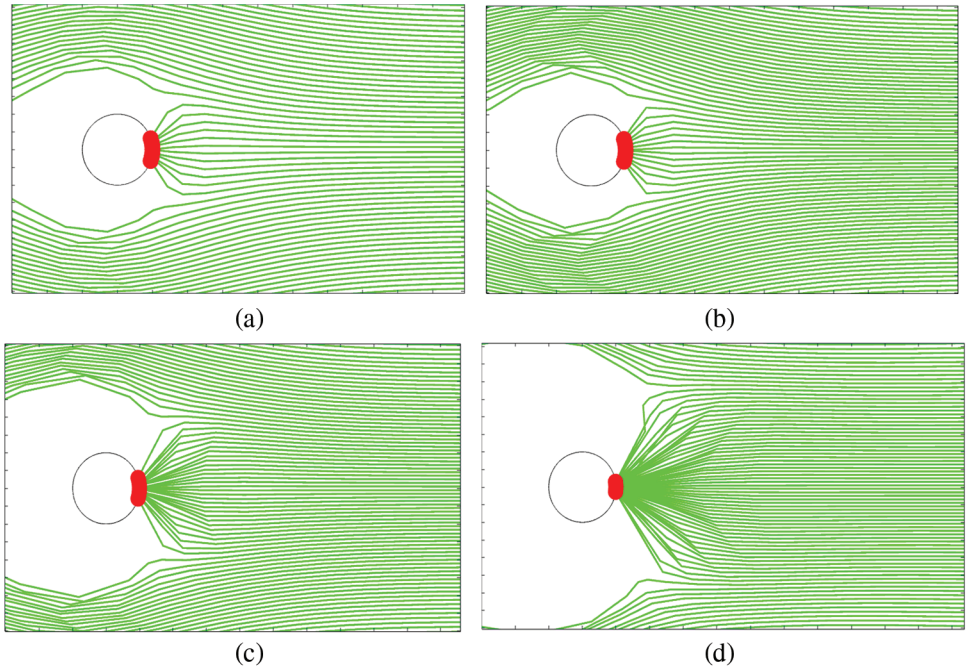

Figure 7: IEAP adsorbed by wire under different dynamic viscosities of slurry (a) η = 0.04 Pa·s, (b) η = 0.0165 Pa·s, (c) η = 0.0047 Pa·s, (d) η = 0.0017 Pa·s

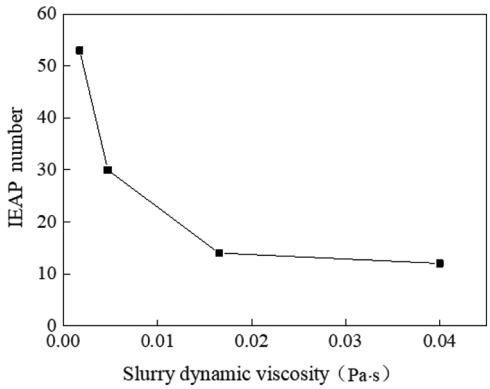

Figure 8: IEAP number at different slurry dynamic viscosities

3.2 Experiment Results and Discussion

3.2.1 Effect of Slurry-Supply Speed on the Number of IEAPs

Fig. 9 shows the experimental results of IEAPs adsorbed by saw wire under different slurry-supply speeds. As slurry-supply speed increases, it can be seen that the number of IEAPs first gradually increases and then ultimately decreases somewhat. Furthermore, fluid drag forces on the abrasive particles

increase as the slurry-supply speed increases. The increase in slurry-supply speed is proportional to the increase of abrasive particle release frequency. This means that more abrasive particles flow to the saw wire when the concentration of abrasive particles in the slurry remains constant. Therefore, more abrasive particles are adsorbed by the saw wire and become IEAPs as slurry-supply speeds increase within a certain range. The fluid drag force is further enhanced with a continuous increase of slurry-supply speed. However, excessive slurry-supply speeds will wash away a significant percentage of the magnetically-adhered abrasive particles, thus resulting in a net decrease in the number of IEAPs adsorbed by the saw wire. As such, even though the release frequency of abrasive particles continues to increase, the net number of IEAPs adsorbed by the saw wire (i.e., the adsorption rate) eventually decreases. These interpretations correspond to the simulation results and thus serve to validate its findings.

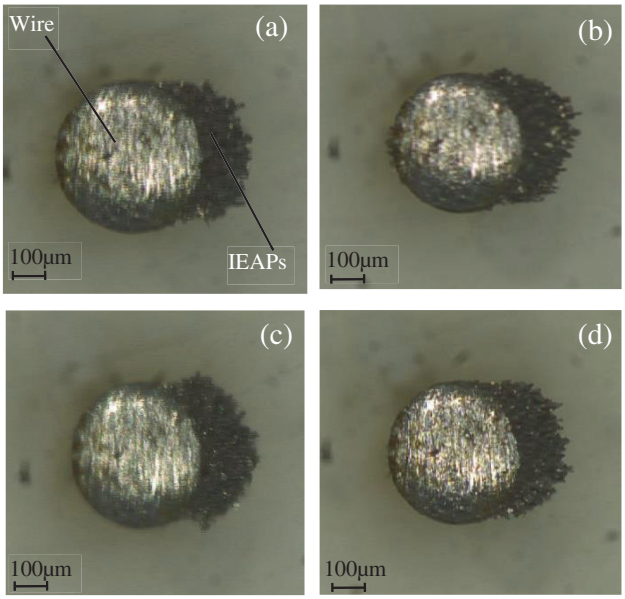

Figure 9: IEAPs adsorbed by wire under different slurry-supply speeds (a) V_0 = 4 mm/s, (b) V_0 = 8 mm/s, (c) V_0 = 12 mm/s (d) V_0 = 16 mm/s

3.2.2 Effects of Slurry Dynamic Viscosity on the Number of IEAPs

Fig. 10 shows the experimental results of IEAPs adsorbed by a saw wire under different dynamic viscosities of slurry. It can be seen that the number of effective abrasive particles adsorbed by the saw wire continues to increase as the cutting fluid's dynamic viscosity decreases. This is mainly because the drag force of abrasive particles continuously decreases as the dynamic viscosity of the cutting fluid decreases. A larger number of abrasive particles are adsorbed by the saw wire to become IEAPs under the condition in which the magnetic forces acting upon the particles remain unchanged. These results are consistent with the reports of Krafcik et al. [18,19], which correspond to the simulation results and thus serve to validate its findings.

3.3 Cutting Experiment Results and Discussion

3.3.1 Effects of Slurry-Supply Speed on Cutting Efficiency

Under this assessment, material-removal-mass per unit time was employed as the evaluation criterion for cutting efficiency. Corresponding cutting efficiencies were then calculated via use of the following formula:

$$\lambda = \frac{m_1 - m_2}{T} \tag{10}$$

where λ is cutting efficiency, m_1 is the mass of the workpiece before cutting, m_2 is the mass of the workpiece after cutting, and T is cutting-time.

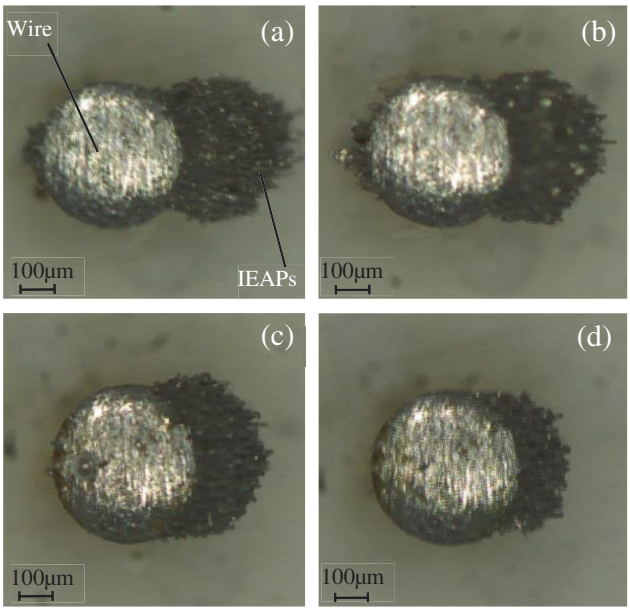

Figure 10: IEAPs adsorbed by wire under different dynamic viscosities of slurry (a) $\eta = 0.0017$ Pa·s, (b) $\eta = 0.0047$ Pa·s, (c) $\eta = 0.0165$ Pa·s, (d) $\eta = 0.04$ Pa·s

Fig. 11 displays cutting efficiency results as a function of varying slurry-supply speeds. In general, it can be seen that cutting efficiency increases more rapidly as slurry-supply speed increases up to about 8 mm/s. The frequency of effective abrasive particles adsorbed by the saw wire increases as slurry-supply speed increases. More abrasives flow to the side of the saw wire, and more IEAPs are brought into the cutting area by the saw wire to participate in cutting; accordingly, the cutting efficiency continues to improve. This is consistent with our previous study [20,21]. However, when the slurry feeding speed reaches about 12 mm/s, the growth trend of cutting efficiency significantly slows down. As slurry-supply speed increases (equivalent to a proportional increase in abrasive particle release frequency), a higher number of abrasive particles tend to flow to the saw wire when the abrasive particle concentration remains constant. Under these conditions, however, the fluidity of grinding-slurry becomes larger. As such, if the slurry-supply speed becomes too high, some IEAPs will be washed away. Moreover, some IEAPs may likewise end up in a non-contact state and would hence not be able to contribute to actual cutting. As a result of the aforementioned mechanisms, the growth trend of wire cutting efficiency would decelerate. These results further corroborate the accuracy of the simulation findings.

3.3.2 Effects of Slurry Dynamic Viscosity on Cutting Efficiency

Fig. 12 shows the results of the functional relationship between the slurry's dynamic viscosity and the cutting efficiency for a workpiece. It was found that the traction force of MAPs decreases as the slurry dynamic viscosity decreases, resulting in a marked increase of the number of effective MAPs adsorbed on the cutting wire. When the slurry dynamic viscosity is 0.0017 Pa·s, the abrasive particles delivered by the viscous forces are minimal. Hence, easy adsorption by the saw wire is not likely, and as a result, the cutting efficiency decreases.

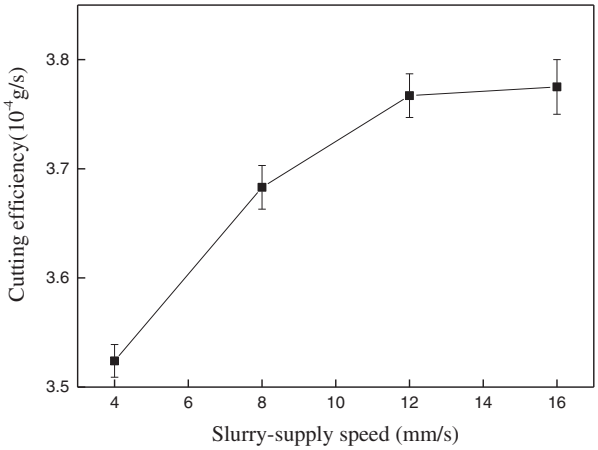

Figure 11: Cutting efficiency under different slurry-supply speeds

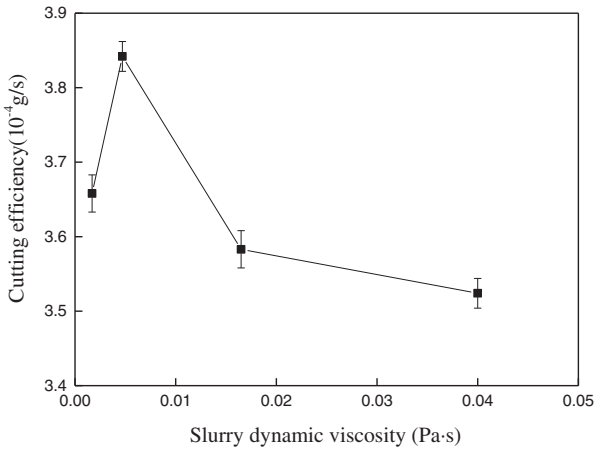

Figure 12: Cutting efficiency under different slurry dynamic viscosities

In the Fig. 12, it can be seen that the cutting efficiency first increases and then decreases, and reaches its maximum value at a dynamic viscosity of 0.0047 Pa·s. The cutting fluid is 100% PEG300 when the dynamic viscosity is at a value of 0.04 Pa·s. At this time, the mixing uniformity of MAPs is optimal. However, the abrasive particles are subjected to significant drag forces because of the large dynamic viscosity at hand along with the poor fluidity of the cutting fluid. The number of IEAPs adsorbed by the saw wire ultimately decreases, resulting in the number of IEAPs entering the cutting area to also become reduced. Hence, the cutting efficiency is at its lowest point when the dynamic viscosity is 0.04 Pa·s. It can also be seen from Fig. 12 that cutting efficiency is generally greater at lower dynamic viscosity values. This is because as the proportion of water increases, the drag force on abrasive particles decreases with a continuous decrease of the cutting fluid's dynamic viscosity. In addition, a mixer is used to continuously stir the slurry to help make the abrasive particles disperse evenly throughout the material; consequently, the number of IEAPs is greatly enhanced. According to the simulation and experimental results, although the abrasive particles brought by drag force are reduced, the number of IEAPs adsorbed by the saw wire is greatly increased. As such, the overall net cutting efficiency depicts a tendency of continuous improvement given the above influential conditions. When the mass fraction of introduced PEG300 is 25% (with the remaining mass in the form of water), the dynamic viscosity is 0.0017 Pa·s. From the perspective of simulation and experimental results, the IEAPs adsorbed by the saw wire accumulate to

their highest level, but the cutting efficiency unfortunately decreases. This is due to the dynamic viscosity of the cutting fluid being very low along with the extent of fluidity being very high. There are very few abrasive particles brought in by the drag force and therefore the particle flow becomes faster, thus leading to a condition in which the MAPs are not easily adsorbed by the saw wire. In addition, the slurry easily produces bubbles during the mixing process, which can also affect the MAPs' ability to be adsorbed by the saw wire (and thus not enter the cutting area). As a result, the cutting efficiency is seen as decreasing under these conditions. In conclusion, the cutting efficiency is highest when the dynamic viscosity of the cutting fluid is 0.0047 Pa·s. Hence, the use of PEG300 can ultimately be reduced to 50% in the endeavor of achieving optimal cutting efficiency, which is conducive to environmental protection and cost reduction.

4 Conclusions

In this study, the formation mechanisms of IEAPs on saw wire surfaces were evaluated both by simulation analysis and experimental trial. In the theoretical analysis, a motion model was built to investigate the IEAP formation mechanisms. It was based on a force analysis of MAPs in a high-gradient magnetic field, which was generated by applying a uniform magnetic field around a saw wire. The formation mechanisms were then investigated via employment of the COMSOL Multiphysics computational module. The results revealed that the number of IEAPs increases with an increase of slurry-supply speed up to about 12 mm/s. The total number of IEAPs adsorbed by the saw wire is at its maximum (i.e., the highest adsorption rate) during a one-second interval when the slurry-supply speed is 12 mm/s. Moreover, the number of IEAPs adsorbed by a saw wire increases as the dynamic viscosity of the cutting fluid decreases.

Direct-observation experiments were primarily conducted to study the effects of different slurry- supply speeds and dynamic viscosities on IEAP formation. The findings were consistent with those obtained from the simulation, which provided validation to the perceived accuracy of the simulation results. Single-wire sawing experiments were conducted to investigate potential effects of different slurry-supply speeds and dynamic viscosities on wire sawing efficiencies. The results showed that the cutting efficiency of workpieces initially increases but then scales back with a decrease in cutting fluid dynamic viscosity. Cutting efficiency is optimized when the dynamic viscosity of the cutting fluid is 0.0047 Pa·s. Under such conditions, the mass fraction of PEG300 is 50%. The deployment of such a fractional concentration of polyethylene glycol in the cutting fluid (as compared to, for example, 100% PEG300) is conducive to protecting the environment and reducing the overall financial costs of silicon wafer production. Cutting efficiency was also found to increase gradually with an increase of slurry-supply speed; however, the growth rate of wire saw cutting efficiency generally slows down as slurry-supply speed continues to rise.

In total, the results of this study provide significant data in the ongoing quest for improving silicon wafer production efficiencies. Such improvements may facilitate substantial cost savings which would prove significantly beneficial to present-day silicon wafer sawing process-related industries.

Funding Statement: This work was funded by the financial support of the NBPT 2021 Research Institute Special Project (NZ21JG004), General Scientific Research Project of Zhejiang Department of Education No. Y202147367.

Conflicts of Interest: The author declares that they have no conflicts of interest to report regarding the present study.

References

1. Wieghold, S., Liu, Z., Raymond, S. J., Meyer, L. T., Williams, J. R. et al. (2019). Detection of sub-500-μm cracks in multicrystalline silicon wafer using edge-illuminated dark-field imaging to enable thin solar cell manufacturing. *Solar Energy Materials and Solar Cells, 196(7),* 70–77. DOI 10.1016/j.solmat.2019.03.033.

2. Ahmed, R., Sreeram, V., Mishra, Y., Arif, M. D. (2020). A review and evaluation of the state-of-the-art in pv solar power forecasting: techniques and optimization. *Renewable and Sustainable Energy Reviews, 124(5),* 109792. DOI 10.1016/j.rser.2020.109792.
3. Nie, S., Kristensen, S. T., Gu, A., Chin, R. L., Trupke, T. et al. (2020). Photoluminescence-based spatially resolved temperature coefficient maps of silicon wafers and solar cells. *IEEE Journal of Photovoltaics, 10(2),* 585–594. DOI 10.1109/JPHOTOV.5503869.
4. Sanamthong, W., Chuti Ma, P. (2020). Chipping size reduction on ultra-thin wafers and narrow saw-streets for wafer sawing process. *Solid State Phenomena, 305(6),* 154–162. DOI 10.4028/www.scientific.net/SSP.305.154.
5. Wang, T. C., Yeh, T. H., Chu, S. Y., Lee, H. Y., Lee, C. T. (2020). Developed diamond wire sawing technique with high slicing ability for multicrystalline silicon wafers. *Materials and Manufacturing Processes, 35(5),* 1–5. DOI 10.1080/10426914.2020.1802037.
6. Costa, E., Xavier, F. A., Knoblauch, R., Binder, C., Weingaertner, W. L. (2020). Effect of cutting parameters on surface integrity of monocrystalline silicon sawn with an endless diamond wire saw. *Solar Energy, 2207(9),* 640–650. DOI 10.1016/j.solener.2020.07.018.
7. Yin, T., Mcl, B., Yu, Z., Yph, D., Wec, B. (2021). Development of an electrolyte jet type apparatus for manufacturing electroplated diamond wires. *Precision Engineering, 68(3),* 351–357. DOI 10.1016/j.precisioneng.2020.12.011.
8. Ge, P., Chen, Z., Wang, P. (2020). Review of monocrystalline silicon slicing technology. *Diamond & Abrasives Engineering, 40(4),* 12–18. DOI CNKI:SUN:JGSM.0.2020-04-004.
9. Bhagavat, S., Kao, I. (2007). Ultra-low load multiple indentation response of materials: In purview of wiresaw slicing and other free abrasive machining (FAM) processes. *International Journal of Machine Tool and Manufacture, 47(3),* 666–672. DOI 10.1016/j.ijmachtools.2006.04.015.
10. Shwinde, S., Berg, M., Kunert, M. (2015). New potential for reduction of kerf loss and wire consumption in multi-wire sawing. *Solar Energy Materials and Solar Cells, 136(5),* 44–47. DOI 10.1016/j.solmat.2014.12.020.
11. Nassauer, B., Kuna, M. (2015). Impact of micromechanical parameters on wire sawing: A 3D discrete element analysis. *Computational Particle Mechanics, 2(1),* 1–9. DOI 10.1007/s40571-015-0036-9.
12. Bao, G., Wang, W., Zhang, L. (2017). Mechanism of material removal in abrasive electrochemical multi-wire sawing of multi-crystalline silicon ingots into wafers. *The International Journal of Advanced Manufacturing Technology, 91(1–4),* 383–388. DOI 10.1007/s00170-016-9718-6.
13. Xie, H., Zou, Y. (2021). Study on the magnetic abrasive finishing process using alternating magnetic field—Discussion on the influence of current waveform variation. *The International Journal of Advanced Manufacturing Technology, 114(5),* 2471–2483. DOI 10.1007/s00170-021-07048-9.
14. Chong, P. H., Tan, Y. W., Yi, P. T., Chong, H. L., Toh, P. Y. et al. (2021). Continuous flow low gradient magnetophoresis of magnetic nanoparticles: Separation kinetic modelling and simulation. *Journal of Superconductivity and Novel Magnetism, 34(8),* 2151–2165. DOI 10.1007/s10948-021-05893-z.
15. Xia, L., Wang, F., Wang, L., Li, X., Chen, J. et al. (2021). Understanding and prediction of magnetization state of elliptic cross-section matrices in high gradient magnetic separation. *Minerals Engineering, 172(10),* 107137. DOI 10.1016/j.mineng.2021.107137.
16. Ren, M., Shu, X. (2020). A novel approach for the numerical simulation of fluid-structure interaction problems in the presence of debris. *Fluid Dynamics & Materials Processing, 16(5),* 979–991. DOI 10.32604/fdmp.2020.09563.
17. Zhang, Q. P., Xue, K., Luo, Y. M. (2020). Structure design and research of magnetic attraction wall climbing robot. *International Core Journal of Engineering, 6(4),* 218–224. DOI P20190813001-202004-202003200001-202003200001-218-224.
18. Krafcik, A., Babinec, P., Babincova, M., Frollo, I. (2019). High gradient magnetic separation with involved basset history force: Configuration with single axial wire. *Powder Technology, 347(3),* 50–58. DOI 10.1016/j.powtec.2019.02.044.

19. Masoud, A., Jafar, J., Mehdi, B. (2020). A computational model for predicting filtration performance of 3D-magnetic filters under different channel geometries, particle sizes and flow conditions. *Colloids and Surfaces A: Physicochemical and Engineering Aspects, 611(10),* 125844. DOI 10.1016/j.colsurfa.2020.125844.
20. Zhang, W., Yao, C. Y., Xu, X. F., Li, H. J., Li, K. (2018). Improvement of magnetic induction-wire sawing process using a magnetic system. *Materials and Manufacturing Processes, 33(6),* 676–682. DOI 10.1080/10426914.2017.1364858.
21. Zhang, W., Qiu, T., Yao, C. (2020). Preparation and optimization of high-purity silicon carbide magnetic abrasives for the magnetic induction-wire sawing process. *Fluid Dynamics & Materials Processing, 16(4),* 709–721. DOI 10.32604/fdmp.2020.010748.